Journal of Medicinal Chemistry

ARTICLE

pubs.acs.org/jmc

Phosphonate−Titanium Dioxide Assemblies: Platform for Multimodal Diagnostic−Therapeutic Nanoprobes

Ivan Řehoř,[†] Vanda Vilímová,[‡] Pavla Jendelová,[§] Vojtěch Kubíček,[†] Daniel Jirák,[∥] Vít Herynek,[∥] Miroslava Kapcalová,[§] Jan Kotek,[†] Jan Černý,[‡] Petr Hermann,[†] and Ivan Lukeš*[,†]

[†]Department of Inorganic Chemistry, Faculty of Science, Charles University in Prague, Hlavova 2030, 128 40 Prague 2, Czech Republic

[‡]Department of Cell Biology, Faculty of Science, Charles University in Prague, Viničná 7, 128 40 Prague, Czech Republic

[§]Department of Neuroscience, Institute of Experimental Medicine ASCR v.v.i., Vídeňská 1083, 142 20 Praha 4, Czech Republic

[∥]Department of Diagnostic and Interventional Radiology, Institute for Clinical and Experimental Medicine, Vídeňská 1958, 140 21 Praha 4, Czech Republic

Supporting Information

ABSTRACT: Multimodal imaging−therapeutic nanoprobe TiO_2@RhdGd was prepared and successfully used for in vitro and in vivo cell tracking as well as for killing of cancer cells in vitro. TiO_2 nanoparticles were used as a core for phosphonic acid modified functionalities, responsible for contrast in MRI and optical imaging. The probe shows high ^1H relaxivity and relaxivity density values. Presence of fluorescent dye allows for visualization by means of fluorescence microscopy. The applicability of the probe was studied, using mesenchymal stem cells, cancer HeLa cells, and T-lymphocytes. The probe did not exhibit toxicity in any of these systems. Labeled cells were successfully visualized in vitro by means of fluorescence microscopy and MRI. Furthermore, it was shown that the probe TiO_2@RhdGd can be changed into a cancer cell killer upon UV light irradiation. The above stated results represent a valuable proof of a principle showing applicability of the probe design for diagnosis and therapy.

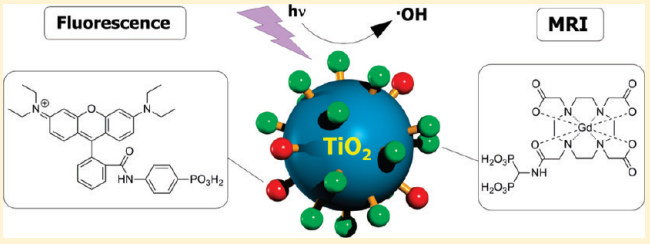

INTRODUCTION

Nanosized objects like inorganic nanoparticles, liposomes, polymers, or other nanovesicles exhibit specific behavior in biological environment.[1] They have prolonged circulation time in the body compared to small molecules. Their ability to penetrate into tissues and effective endocytosis is documented. They possess the ability to accumulate in tumor tissue because of the enhanced permeability and retention (EPR) effect.[2] Nanovesicles can also carry considerably higher payload of a contrast agent or a drug compared to low-molecular structures. Therefore, using nanoobjects for preparation of advanced medical agents is very advantageous.

Unique biological properties stated above led to use of a wide spectrum of nanoscale objects for preparation of contrast agents (CA) for various medical imaging modalities including magnetic resonance imaging (MRI),[3,4] radiomethods,[5] optical imaging (OI),[6] and others. The combination of various functions into one agent gives rise to multimodal imaging and imaging−therapeutic probes. The presence of two or more agents in one probe ensures their identical biodistribution and allows for combining of advantages of particular imaging techniques. Combination of MRI and optical imaging in one MRI−OI probe is particularly useful. MRI has exclusive spatial resolution but rather poor sensitivity and specificity. On the other hand, optical imaging has excellent sensitivity and very good resolution, but the depth of detection is its limiting factor. Combined MRI−OI agents have great application potential in selective tumor labeling for oncological diagnosis and surgery.[7,8] This class of probes can be also effectively used for cell labeling, for example, during stem cell transplantations.[9]

Nanosized multimodal medical probes with inorganic nanoparticle core were widely studied. Molecules responsible for various probe functions are usually attached onto the nanoparticle surface or are incorporated into the nanoparticle structure. Several types of nanoparticles can provide specific functions themselves (i.e., quantum dots active in optical imaging, magnetic nanoparticles active in MRI, nanoparticles consisting of drug molecules, etc.).

Most MRI−OI imaging nanoprobes are based on superparamagnetic iron oxide nanoparticles. These probes provide a negative signal in MRI; i.e., their presence is indicated by hypointense area in T_2 weighted images (negative, T_2 contrast). Sometimes these areas can be difficult to distinguish from other signal voids and a loss of spatial resolution is occurring in the presence of CA.[10] Another approach is represented by attachment of Gd complexes on a diamagnetic core. Presence of Gd chelates results in a hyperintense area in T_1 weighted images

Received: April 14, 2011
Published: June 12, 2011

(positive, T_1 contrast) and lacks the listed disadvantages of superparamagnetic nanoparticles. Nevertheless their sensitivity is lower than that of superparamagnetic nanoparticles. Accumulation of a number of CA molecules in one entity helps to overcome the MRI sensitivity problem. Furthermore, the r_1 relaxivity expressing the efficiency of MRI CA is increased upon attachment because of the slowing of the tumbling of the chelate in solution.[11]

The reported T_1 MRI and OI active inorganic nanoparticles use the cores consisting of fluorescent dye-doped silica,[12] zeolite,[13,14] nanoparticle, or quantum dots[15] (usually coated by silica shell[16−18]). The surface architecture, containing Gd chelates, is usually created using silyl ester chemistry. Hydrolysis of silyl ester modified molecules performed in dispersion containing nanoparticles leads to their grafting onto the surface.[12] An alternative is nanoparticle modification with aminopropyltrialkoxysilane and consequent treatment of surface amino groups with Gd chelates, typically using amidic coupling techniques.[13] In either case, the surface of the particle consists of R-SiO_3 units. The low resistance of this surface architecture against hydrolysis is well described.[19] An alternative to overcoming the problem of hydrolytical lability is the creation of liposome-like bilayers around lipid coated silica particles.[16,18]

Titanium dioxide is an inert and nontoxic material, and thus, it was utilized for preparation of MRI[20] and luminescence[21] imaging nanoprobes. However, when TiO_2 is irradiated with UV light, electron excitation occurs and the electron or/and its energy can be transferred to another molecule and be responsible for chemical changes. Irradiated TiO_2 in aqueous solution produces highly toxic ·OH radicals. Therefore, TiO_2 nanoparticles are effectively used for disinfection in water treatment[22,23] and it appears that these properties can also be used for killing of cancer cells.[24−29]

Recently, we published a paper describing the preparation and promising MRI properties of TiO_2 nanoparticles covered with phosphonated Gd chelates.[30] Consequently, we performed a study on adsorption properties of phosphonic and geminal bisphosphonic acids onto the surface of nanocrystalline TiO_2.[31] This study revealed that bisphosphonate strongly interacts with the surface. The interaction results in formation of a coordination polymer consisting of -P-O-Ti-O-P- chains, which covers the surface of nanoparticle. Extremely high loads of bisphosphonate (almost 4 times higher than that corresponding to monolayer surface coverage) indicate creation of polymeric 3D structures forming multilayers on the surface. These multilayers exhibit extremely high stability against desorption, even in the presence of competing sorbate (phosphate buffer). Furthermore, it was found that bisphosphonate and phosphonate can be coadsorbed together, giving rise to similar bisphosphonate multilayers with incorporated phosphonate. These outstanding properties led us to exploit the TiO_2−phosphonic acid scaffold for the preparation of a multimodal nanoagent, presented in this work.

The preparation of the bimodal MRI−OI probe proceeds in one pot by single step coadsorption of both sorbates in an aqueous solution. The developed method allows for preparation of monodisperse nanocolloids of 12 nm anatase nanoparticles modified with phosphonates and geminal bisphosphonates, which are stable under biological conditions. The results prove that the procedure is simple and universal and could lead to large scale production of TiO_2 nanoprobes covered with molecules of various contrast agents. The application potential of the probe for cell labeling is tested on stem cells, HeLa human cancer cells, and T-lyphocytes, which were labeled and visualized by fluorescence microscopy and by MRI. Furthermore, the viability of the human HeLa cancer cells incubated in the presence of our nanoagent was followed upon UV irradiation.

Scheme 1. Structures of Discussed Molecules

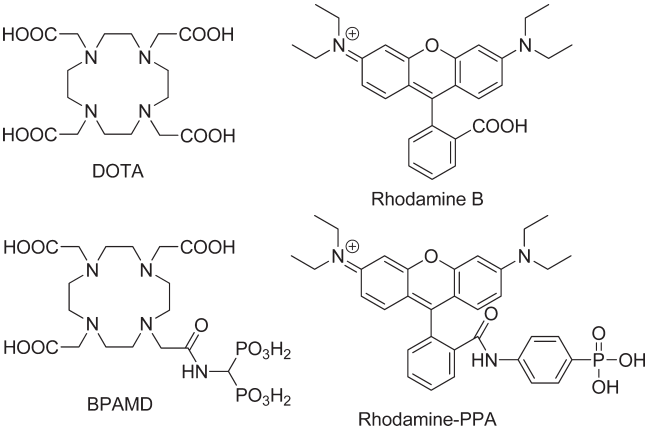

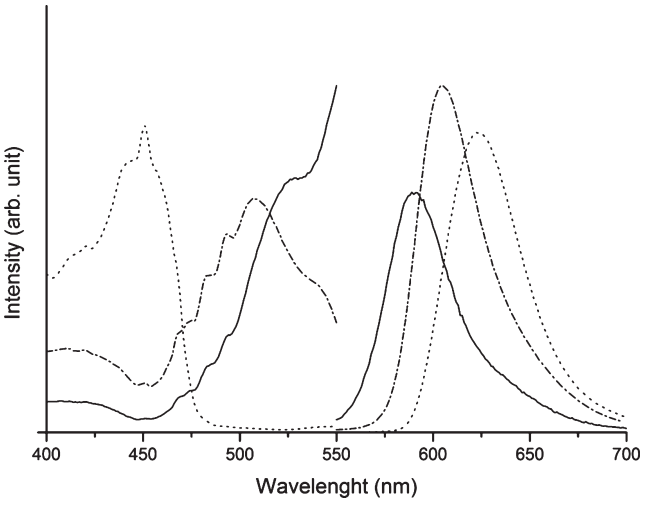

Figure 1. Excitation (left part of the plot) and emission (right part of the plot) spectra of rhodamine B (dotted line), rhodamine−PPA (dash-dotted line), and TiO_2@RhdGd (solid line). The intensities of the signals are relative and are given by the measurement conditions for each sample.

RESULTS AND DISCUSSION

Preparation and Properties of Covering Molecules. Macrocyclic ligand BPAMD, containing geminal bisphosphonate in the pendent arm (Scheme 1), was prepared in our laboratory.[32] The structure of the ligand is derived from the ligand DOTA (Scheme 1), whose Gd complexes are used as MRI contrast agent (CA) in clinical practice. The bisphosphonate group remains uncoordinated and is free for interaction with solid substrates[33] or metal ions.[34] The relaxation properties of Gd-BPAMD are within the range expected for DOTA-like complexes.[35] Lanthanide complexes of BPAMD exhibit high stability, and thus, no decomplexation has been observed under

conditions of adsorption reaction according to NMR and fluorescence experiments.[31]

Among many existing fluorescent dyes, rhodamine B was chosen for several reasons: (i) it is water-soluble, and therefore, the surface of modified particles remains hydrophilic (hydrophobization of the nanoparticle surface can lead to loss of colloidal stability); (ii) its emission wavelength is in the red part of the spectra, ensuring good tissue penetration; (iii) rhodamine B is a widely used dye, and most fluorescence microscopes can be tuned to its excitation and emission parameters.

The conjugate of rhodamine B and phenylphosphonic acid (rhodamine−PPA, Scheme 1) was prepared from rhodamine B and diethyl 4-aminophenylphosphonate. Excess of coupling agent had to be used in the first reaction step to achieve 70% conversion. The second reaction step proceeds quantitatively, and no purification of the product was necessary. The change of luminescent properties occurs upon modification of the rhodamine B (Figure 1). The excitation band moves 60 nm to the longer wavelength, and the emission band moves 20 nm to the lower wavelength.

Preparation and Properties of Nanoprobe TiO_2@RhdGd. Acid-stabilized colloidal TiO_2 (anatase, 12 nm diameter) was used as a substrate for adsorption. The adsorption reaction of both sorbates Gd-BPAMD and rhodamine−PPA onto the TiO_2 nanoparticles was performed in one reaction step. The adsorption reaction proceeds under acidic conditions. The procedure, involving several dialysis cycles and addition of polyvinylalcohol (PVA), was developed to remove excess sorbate and to obtain modified material as a colloid of concentration, 2.1 mg TiO_2@RhdGd per milliter, stable at neutral pH. The procedure led to completely transparent colloids with pH ∼6.5. Prepared samples were stable in water, physiological solution (0.9% NaCl, pH 7.4), and cell incubation solution.

The detailed methodology of sample preparation and the study of adsorption properties of phosphonate and bisphosphonate and of their coadsorption were recently published by our team.[31] The study shows that adsorption of bisphosphonates leads to formation of hydrolytically stable multilayers on the surface. When bisphosphonate and phosphonate are coadsorbed, phosphonate molecules are incorporated into this multilayer structure. These results were also confirmed for TiO_2@RhdGd, and their discussion can be found in Supporting Information. The amount of Gd-BPAMD in TiO_2@RhdGd was estimated using ICP-AES to be 1.22 mmol of Gd-BPAMD per 1 g of TiO_2. The amount of adsorbed rhodamine-PPA, 0.18 mmol per 1 g of TiO_2, was estimated indirectly by determination of its content in dialyzing solutions by means of UV−vis spectroscopy.

Quantification of the amount of adsorbates shows that the complex is approximately 6.6 times more abundant on the surface than fluorescent dye. Surface covered mainly with MRI contrast agent molecules is a rational design of probe, as the sensitivity of MRI is much lower than the sensitivity of OI.

The MRI properties of the prepared nanoprobe were studied. A plot of millimolar r_1 relaxivity (corresponding to the MRI efficiency) vs magnetic field is given in Figure 2. Significant millimolar relaxivity increase in comparison with free Gd-BPAMD complex is observed. Also, the shape of the curve changes and exhibits a maximum (28 mM^{-1} s^{-1}) at 20 MHz. The relaxivity increase and the presence of a local maximum are attributed to the immobilization of chelates on the surface, which causes prolongation of a rotational correlation time.[11] High

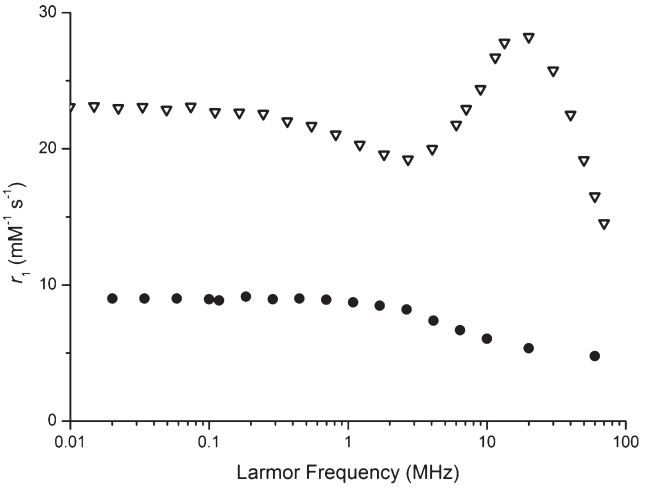

Figure 2. ^1H NMRD profiles of the Gd-BPAMD complex in solution (circles) and TiO_2@RhdGd colloid (triangles) (measured at 25 °C).

relaxivity values indicate that even though multilayers of covering molecules are present on the surface, these layers are well hydrated and water molecules can effectively approach Gd(III) complexes. The number of the Gd(III) chelates adsorbed on one 12 nm nanoparticle was calculated to be around 4800. Therefore, r_1 relaxivity per one particle can be calculated as approximately 135 000 $mmol^{-1}$ s^{-1} (20 MHz, 25 °C). The calculation is described in Supporting Information.

The relaxivity per mM Gd(III) solution (28 $mM^{-1}s^{-1}$, 20 MHz, 25 °C) can be recalculated into so-called density of relaxivity,[36] i.e., relaxivity per 1 g of contrast agent dissolved in 1 L of water. The value 18.2 s^{-1} $g^{-1}dm^3$ is almost 3 times higher than value 6.7 s^{-1} $g^{-1}dm^3$ reported for GdDOTA, MRI CA commonly used in human medicine. The doses of MRI CAs used in clinical practice are in gram scale, and therefore, the relaxivity value expressed with respect to weight of contrast agent is crucial for considering its applicability.

Excitation and emission spectra of the prepared probe were measured (Figure 1). The excitation band is moved to the longer wavelengths in comparison with rhodamine−PPA and is influenced by scattering on the colloid particles at longer wavelengths. The emission band is moved even more to the shorter wavelengths ($\lambda_{Em,max}$ = 591 nm) than in the case of rhodamine−PPA.

Labeling of Stem Cells. Stem cells have ability to undergo mitosis and to differentiate into cells of specific tissue. For this ability, stem cells are used in cell therapy, a very perspective branch of modern medicine research, where transplantation of stem cells into damaged tissue leads to its reparation. Tracking of the cells during and after the transplantation process is essential for understanding the process as well as for successful treatment. MRI is a particularly suitable technique for such tracking.[37,38] As a model for testing the suitability of our bimodal probe for stem cells labeling, we have chosen rat mesenchymal stem cells (rMSCs) as an example of adult stem cells, since they are easily derived from bone marrow, can differentiate into a variety of specialized cell populations, and are efficiently proliferated in vitro. The results concerning stem cells viability are of particular importance, as stem cells are very sensitive toward the presence of any chemical and therefore can serve as a very good test of probe biocompatibility.

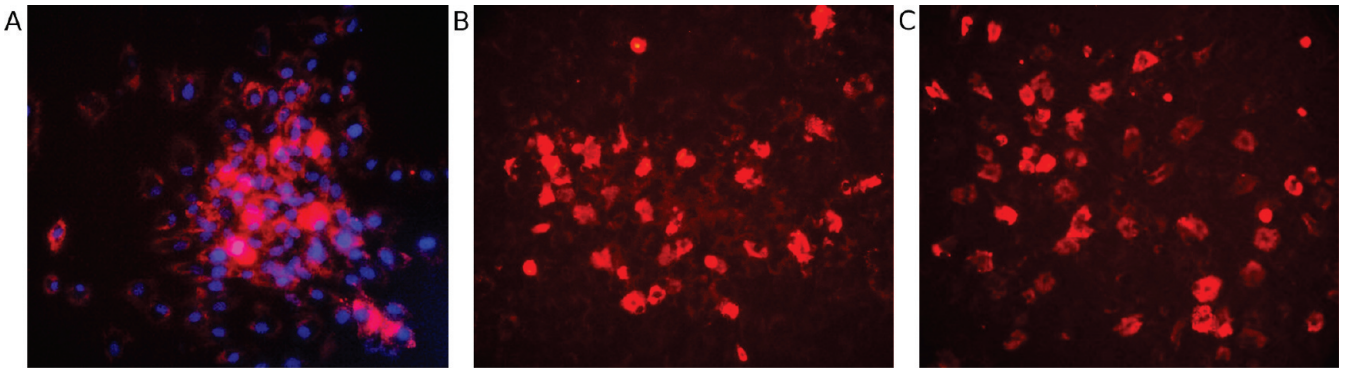

Figure 3. Image of labeled rMSCs, obtained by fluorescence microscopy: (A) TiO_2@RhdGd-labeled MSCs (red) with cell nuclei colabeled with DAPI (blue); (B) image obtained immediately after 48 h of incubation with TiO_2@RhdGd agent; (C) image obtained 7 days after the contrast agent was washed out. Cell nuclei were not colabeled to avoid affecting cell viability. Scale bar, 50 μm.

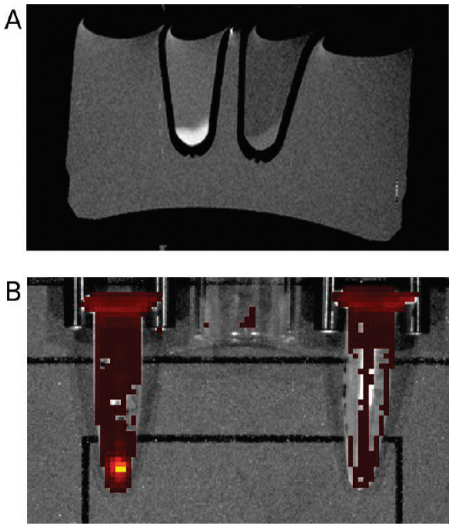

Figure 4. Visualization of rat mesenchymal stem cell suspensions: (A) magnetic resonance image of vials with labeled cells (left) and control unlabeled ones (right); (B) fluorescence from labeled cells (left) and control unlabeled ones (right).

The cells were labeled by cultivation for 48 h in medium containing TiO_2@RhdGd agent. After incubation, the cells were washed with culture medium. The viability of rMSCs labeled with TiO_2@RhdGd agent was not affected, reaching 95% and suggesting the biocompatibility (nontoxicity) of TiO_2@RhdGd agent. Also, the growth of cells in comparison with an unlabeled control was not affected. The labeling efficiency was determined by fluorescence microscopy (Figure 3A), which showed that more than 89% of cells was labeled. To check the possible efflux of the internalized TiO_2@RhdGd agent out of the cells, the labeled cells (Figure 3B) were cultured for another 7 days in medium not containing TiO_2@RhdGd. Even after this period of time the labeled cells were very well visible via fluorescence microscopy (Figure 3C).

Labeled cells were harvested, and their suspensions were centrifuged in vials to form a pellet on the bottom on the vial. A T_1-weighted MRI slice through the settled cells showed a noticeable contrast between suspensions of the labeled and the control cells (Figure 4A). a fluorescence camera was also used for labeled cells visualization. The image of capillary with labeled and unlabeled cells showed intensive, easily detectable fluorescence (Figure 4B). The above stated results show very good labeling ability of our probe as well as long persistence inside the cells.

To confirm the results obtained from rat MSCs and to prove nontoxicity of our probe in more clinically relevant cell model, we performed real time cell proliferation analysis using RTCA Instrument on human mesenchymal stem cells. Cells were seeded in E-Plates 16. The solution of TiO_2@RhdGd was added to cells after 6 h, i.e., in the proliferation curve plateau. The cells in the second experiment were incubated in the presence of TiO_2@RhdGd from the beginning. There is no effect of probe presence on cell proliferation and viability observed (for plots see Supporting Information), indicating any cytotoxic effect on hMSC. The labeling efficiency of hMSCs was 82%, i.e., was comparable with results obtained with rMSCs.

Labeling of HeLa cells. It is well described that nanoscale objects are accumulated in solid tumors because of the enhanced permeability and retention (EPR) effect.[2] As our probe is a typical nanoparticle of a significant size, it is expected to accumulate in cancer tissue. Accumulation in the solid tumor is the only prerequisite for efficient antitumor activity. There must also be efficient entry of the potential anticancer substance/nanoparticle into the cell. Therefore, pilot experiments studying the interaction of TiO_2@RhdGd with a typical human adenocarcinoma cell line were performed (HeLa). The experiments were designed to prove the ability of TiO_2@RhdGd to enter the cells, the vesicular pathway of storage and accumulation inside the cell, and also the ability to kill cancer cells containing TiO_2@RhdGd upon UV irradiation.

Although our probe did not exhibit toxicity on sensitive stem cells, the viability experiments on HeLa cells, which are much more robust and less sensitive to various substances toxic to the primary cell lines, were also performed, as potential toxicity can distort interpretation of appropriate results. Cells were incubated in medium containing TiO_2@RhdGd. DAPI (impermeable into the normal live cells) was used for identification of the damaged/dead cells. The numbers of living and dead cells were quantified using flow cytometer and compared to control group, incubated in the absence of TiO_2@RhdGd. The viability of HeLa cells was not influenced by the presence of TiO_2@RhdGd and was about 96% in all samples.

Nanoparticles typically enter the cell via endocytosis using various types of endosomes. Following their trafficking inside the cell is crucial for the predictions of the time they spend inside the

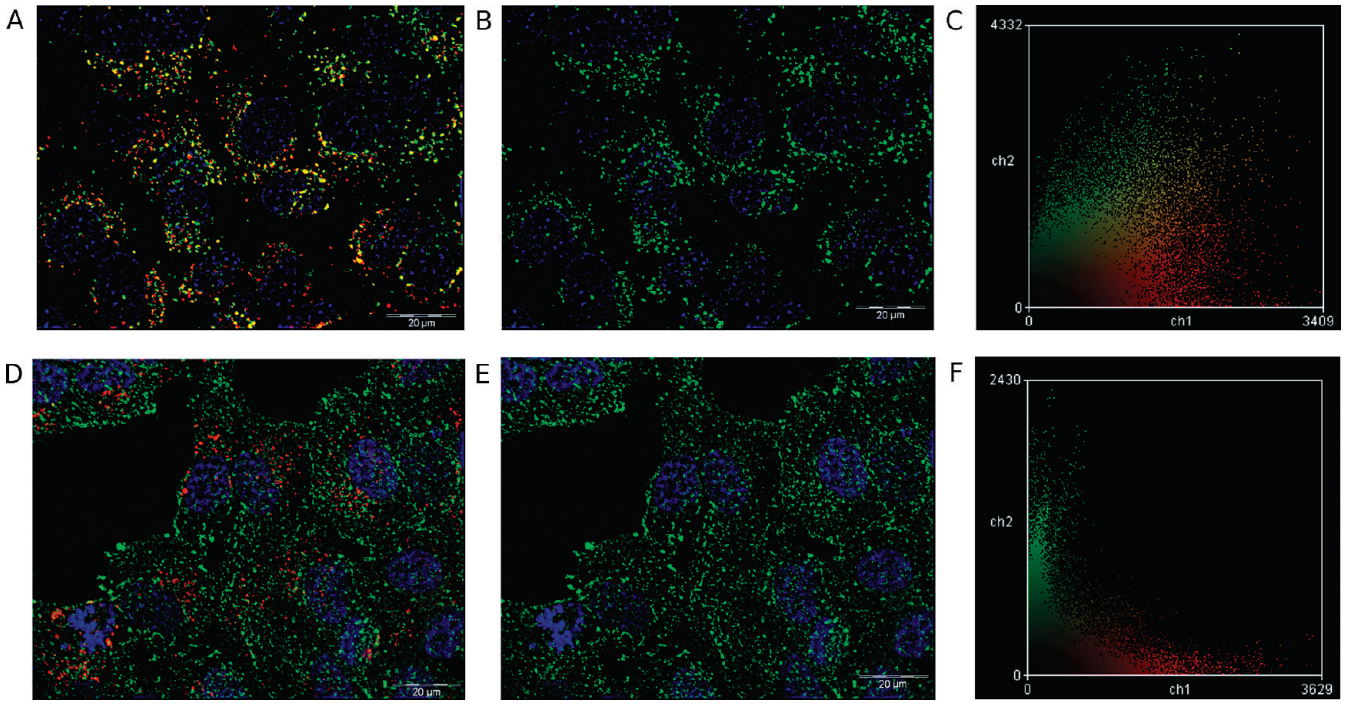

Figure 5. Fluorescence microscopy, colocalization of nanoparticles with holotransferrin-FITC and lysosomal marker LAMP-1, nuclei stained with DAPI (blue) in all images: (A) colocalization of nanoparticles (red) with LAMP-1 (green) in HeLa cells; (B) lysosomal pattern of LAMP-1 staining only (green) in HeLa cells (displayed same sample location as in (A); (C) colocalization plot (intensity of pixels in both color channels) between nanoparticles (red) and LAMP-1 specific staining (green) exhibiting extremely high colocalization values; (D) colocalization of nanoparticles (red) and holotransferrin-FITC (green) in HeLa cells; (E) localization of hotransferrin-FITC (green) in HeLa cells, typical pattern of early and recycling endosomes (displayed same sample location as in (D)); (F) colocalization plot between nanoparticles (red) and holotrasferrin-FITC exhibiting lack of colocalization.

cell before are cleared away. Therefore, we performed the colocalization studies of the fluorescence signal from internalized nanoparticles with typical markers of early and recycling endosomes (fluorescently labeled holotransferrin) and, in separate experiment, of lysosomes (anti-LAMP-1 antibody) as shown in Figure 5.

The obvious overlap between the fluorescence signals of nanoparticles and Lamp-1 in Figure 5A indicates localization of nanoparticles inside the lysosomes. The colocalization is formalized in Figure 5C, where the fluorescence of TiO_2@RhdGd is localized on the *x* axis while the LAMP-1 fluorescence is localized on the *y* axis. It is obvious that most of the individual fluorescent events exhibit both types of fluorescence; i.e., most of the signal density is localized in the middle of the diagram. In contrast, the position of fluorescence signals of TiO_2@RhdGd does not correspond to the signals of holotransferrin-FITC (Figure 5D,E). Again, quantitative information is very visible in the diagram in Figure 5F, where the majority of the signal density is distributed along the *x* and *y* axes, indicating that only a negligible amount of TiO_2@RhdGd is localized in early and recycling endosomes.

The results from colocalization experiments show that nanoparticular probe is localized exclusively in lysosomes. This means that nanoparticles follow the endocytic pathway, and so they are not excluded from the cell via recycling endosomes. Therefore, one can find them accumulated in terminally differentiated lysosomes (the same behavior is exhibited by dextrane probes widely used to mark lysosomal compartment). A small amount of nanoparticles localized in endosomes (colocalizing with the holotransferrin) probably belongs to the ongoing endocytic events indicating the entry pathway for the particle internalization. The results of these experiments are in a good agreement with experiments on stem cells, where 1 week after incubation only negligible nanoparticle clearance was observed. Successful internalization and long-term storage of nanoparticles inside the cells increase their value as biomedical probes and spread the possibilities of their application. TiO_2@RhdGd nanoparticles could be used in some special applications as nontoxic fixable probes for lysosomes useful for in vivo imaging.

Photocatalytic Activity of TiO_2@RhdGd Used for Killing of HeLa Cells. The tests of photocatalytical activity leading to cancer cell death were performed for TiO_2@RhdGd. HeLa cells were incubated in medium containing TiO_2@RhdGd, were extensively washed with phosphate buffer, and were illuminated with UV light. The absorption edge of TiO_2 is around 360 nm. As the toxicity of UV light increases with decreasing wavelength, the filter from the soft glass (Petri dish) was used to filter off wavelengths under 350 nm. The irradiation was performed for 7−20 min. For precise estimation of destructive UV impact, including delayed effects, cells were incubated for another 3 h after illumination. Viability of harvested cells is plotted in Figure 6. The plot shows that cells labeled with nanoparticles are dying much more in longer exposure times than the cells in the control group; however, the population in the control group also suffers from UV exposure.

Still the penetration depth of UV light in tissue is very small (it is estimated to be less than 0.1 mm, whereas the typical penetration depth in living tissue of the red light used for photodynamic therapy ranges between 1 and 3 mm) and a shift

dx.doi.org/10.1021/jm200449y |*J. Med. Chem.* 2011, 54, 5185–5194

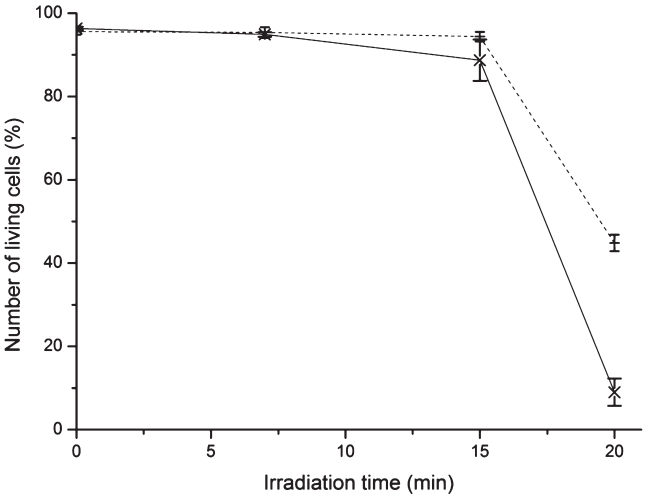

Figure 6. Viability of UV illuminated cells, incubated in the presence of TiO_2@RhdGd (×, full line) and comparison with control group (+, dashed line). Experiment was performed in triplicate; errors are expressed in form of standard deviation.

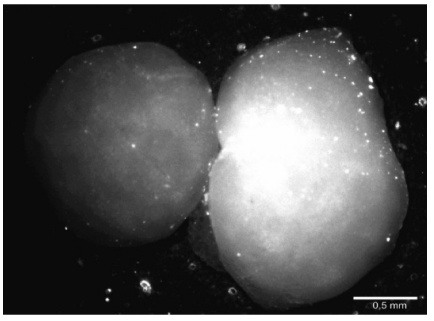

Figure 7. Mice inguinal lymph node containing splenocytes labeled with TiO_2@RhdGd (right) and control lymphnode (left). Image obtained from fluorescence binolupe.

of this wavelength into the visible range of spectra using a suitable chromophore is a challenging task, allowing effective use of the prepared system in vivo.

Homing of TiO_2@RhdGd Labeled Leukocytes in Vivo. As was shown and discussed before, TiO_2@RhdGd probe is nontoxic, is efficiently endocytosed, enters the lysosomal storage compartment, and can potentially label the appropriate cell for the long period. We also tested the potential of the TiO_2@RhdGd to become a long-term probe for bimodal (MRI/fluorescence) labeling of migratory cell populations in vivo. We decided to use cell suspension derived from lymph nodes to test the hypothesis that primary leukocytes treated in vitro with TiO_2@RhdGd can be introduced back into the recipient animal and that these cells are able consequently to home and find their appropriate locations in situ in the secondary lymphoid organs. The cells derived from lymph nodes are complex suspensions (composed mostly of T-lymphocytes, together with B-lymphocytes and antigen presenting cells) containing cells with high endocytic rates. Figure 7 shows that cells endocytosed TiO_2@RhdGd probe in vitro and after injection into the caudal vein were able to home into the original location, i.e., the lymph node. Microscopic investigation of

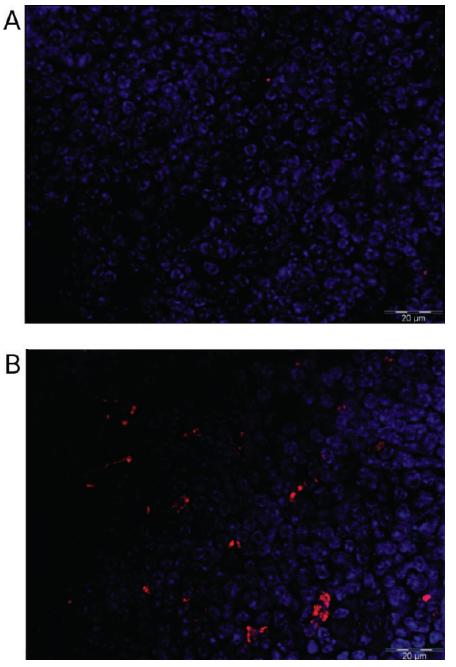

Figure 8. Fluorescent microphotography of cryocut lymph nodes from control mouse (A) and from the mouse with injected TiO_2@RhdGd labeled lymph node derived cells (B). Red signal indicates fluorescence of TiO_2@RhdGd accumulated in lysosomal compartment of homed leukocytes. Blue signal indicates nuclei labeled with DAPI.

cryocuts prepared from inguinal lymph nodes (obtained from control mouse and from mouse injected with the TiO_2@RhdGd treated cell suspension derived from lymph nodes) clearly showed that TiO_2@RhdGd treated cell population injected into recipient mouse was able to home back to lymph node. This ability was not altered by TiO_2@RhdGd and the cells could be visualized using fluorescence microscopy (Figure 8).

CONCLUSION

A novel dual MRI + OI nanoprobe also showing photoactive properties was synthesized and tested for living systems. The probe core consists of a TiO_2 nanoparticle, and its surface is covered with Gd(III) chelates responsible for contrast in MRI and fluorescent rhodamine B derivatives. The Gd(III) chelator contains the bisphosphonic acid group in the side chain, and rhodamine contains the phosphonic acid group. Through the phosphorus functionalities, the MRI and optical imaging contrast agents were linked to the surface of TiO_2 nanoparticles. This functionalization proceeds in aqueous medium and allows for grafting of both functionalities onto the surface in one step. The formation of well hydrated multilayers of bisphosphonate−Ti coordination polymers on the surface is responsible for very high loads of modifying molecules; however, these remain accessible from the solution. The bisphosphonate covers exhibit very high hydrolytical stability, which allows application of the nanoprobe for long-term tasks in the human body. The prepared MRI−OI probe has excellent relaxivity as well as relaxivity density, and the fluorescence intensity is sufficient for observation of probe behavior in living systems.

Three types of cells were used in our study: mesenchymal stem cells, adenocarcinoma HeLa cells, and cells derived from the lymph node. The probe did not exhibit toxicity in any of these

systems. The nanoprobe penetrates into the cells in an amount sufficient for cell tracking. In the case of HeLa cells, storage in the lysosomal compartment was confirmed. Furthermore, it was shown that the TiO_2@RhdGd remains inside the cells for a number of days, which is essential for cell tracking applications.

The core of the probe, a photoactive TiO_2 nanoparticle, although is inert under normal conditions, upon UV irradiation produces highly toxic ·OH radicals, which can cause the death of the surrounding living tissue. In an experiment with cancer HeLa cells, we demonstrated that nontoxic, biocompatible probe TiO_2@RhdGd can be changed into a cancer cell killer upon UV light irradiation. The TiO_2@RhdGd probe was designed to possess MRI and fluorescence, diagnostic modalities that allow exact tumor localization. When exact tumor position is known, the UV irradiation can be performed directly in the place of the tumor, avoiding shielding from surrounding tissue. We have performed experiments proving that the probe can visualize tissues via MRI and fluorescence, as well as kill cancer cells under in vitro conditions.

EXPERIMENTAL SECTION

Materials. Diethyl 4-aminophenylphosphonate and ligand BPAMD (Scheme 1) and its complexes were prepared according to the published procedures.[30,32,39] Nanocrystalline anatase (average particle diameter 12 nm) was used as a sorbent.[40] The material was used in the form of stable transparent colloidal solution (pH ∼2.5, TiO_2 concentration of 1.8 g/L according to ICP-AES, specific surface ∼180 m^2/g). Polyvinyl alcohol (M_w = 80 kDa, 86−89% hydrolyzed, Wacker) was used for colloid stabilization. Standard grade chemicals and deionized water were used for adsorption and desorption experiments; for the preparation of ICP samples, high-purity grade sulfuric acid, nitric acid, hydrogen peroxide, and reverse osmosis purified water were used.

Dialysis. An ultrapor membrane with cutoff of 6−8 kDa was used for dialysis. The ratio between volumes inside the membrane and the washing medium was 1:250 for all experiments. One dialysis step was performed for 12 h. The dialyzing solution was stirred.

MS. Mass spectra were acquired on a Bruker Esquire 3000 spectrometer equipped with an electrospray ion source.

NMR. ^{1}H (399.95 MHz), ^{13}C (100.58 MHz), and ^{31}P (161.9 MHz) NMR spectra were acquired at 25 °C (unless stated otherwise) with a Varian Unity Inova-400 spectrometer, using 5 mm sample tubes. For the ^{1}H and ^{13}C measurements in D_2O, the methyl signal of *t*-BuOH was used as an internal standard (δ = 1.2 and 31.2 ppm, respectively). The ^{31}P chemical shifts were measured with respect to 1% H_3PO_4 in D_2O as an external reference.

ICP-AES. The concentrations of Gd and Ti were determined with an ICP-AES spectrometer VistaPro (Varian) in axial plasma configuration, equipped with an autosampler SPS-5, an inert parallel flow nebulizer, an inert spray chamber, and a demountable torch with an inert injector tube. The samples (200 uL) were digested in concentrated H_2SO_4 (300 uL) and concentrated H_2O_2 (100 μL) at 170 °C for 24 h. For measurement, the solutions were diluted with 1% HNO_3 to a volume of 10 mL.

UV−Visible. The concentration of rhodamine−PPA in dialyzing solutions was determined with a Unicam UV300 UV/vis spectrophotometer using 1 cm quartz tubes. Dialyzing solutions (1 L each) were concentrated using rotary evaporator to approximately 100 mL each. The obtained solutions were mixed and concentrated using rotary evaporation to 71.5 g. The pH of the resulting sample was 1.4. Absorbance of the sample was measured at 570 nm.

TEM, HR-TEM. The morphology and size of the particles were investigated by means of TEM (TecnaiG2 SpiritTwin 12, 120 kV) and HRTEM (Jeol JEM 3010, 300 kV), for which a drop of diluted sample was placed on a carbon coated copper grid (SPI 3630C-MB) and was left to dry freely.

Luminescence. The luminescence measurements were performed on an Edinburgh Instruments FS900 spectrofluorimeter, equipped with a 450 W xenon arc lamp, a microsecond flash lamp, and a red-sensitive photomultiplier (300−850 nm).

^{1}H Relaxivity. Relaxivities were measured on a Bruker Minispec MQ20 relaxometer (Bruker, Germany; 20 MHz, 25 °C). The NMRD profile was measured on a Stelar FFC spectrometer operating at 0.01−20 MHz and a Stelar SpinMaster spectrometer operating at 20−70 MHz.

Fluorescence Microscopy. The cells were visualized using an Olympus IX81 CellR fluorescence microscope equipped with a Hamamatsu C4742-80-12AG digital camera under a 63× oil-immersion lens and Tx Red (572 mn), DAPI (350 mn), and GFP filters (540 mn).

Optical Imaging. Optical imaging was performed using a Caliper IVIS Lumina XR imager (used excitation wavelength 535 nm).

Preparation of Rhodamine−PPEt$_2$ Conjugate. Diethyl 4-aminophenylphosphonate (96 mg, 0.42 mmol) was mixed with dimethylaminopyridine (100 mg, 0.82 mmol), 1-(hydroxy)benzotriazole (HOBT) (56 mg, 0.57 mmol), *N*,*N*-(diisopropyl)ethylamine (110 mg, 0.85 mmol), and [9-(2-carboxyphenyl)-6-diethylamino-3-xanthenylidene]diethylammonium chloride (rhodamine B) (200 mg, 0.42 mmol). The mixture was dissolved in dry MeCN (20 mL), and powder *N*,*N*,*N*′,*N*′-tetramethyl-*o*-(benzotriazol-1-yl)uronium tetrafluoroborate (TBTU, 540 mg, 1.68 mmol) was added. The reaction mixture was stirred at room temperature in the dark for 12 h. The solvent was evaporated on a rotavap, and the product was purified by column chromatography on silica (mobile phase of EtOAc/AcOH/EtOH = 100:2:5 {vol}; R_{ef} = 0.5). Crude product, containing remains of HOBT and diethyl 4-aminophenylphosphonate, was purified by column chromatography (mobile phase of CH_2Cl_2/MeOH = 20:1) to obtain pure product in the form of a purple oil (yield 140 mg, 51%). ^{1}H NMR (CD_3OD): δ = 1.11 ppm (12H, t, CH_3-CH_2-N), 1.22 (6H, td, CH_3-CH_2-O), 3.33 ppm (8H, q, CH_2-N), 4.00 ppm (4H, m, CH_2-O), 6.30 ppm (2H, d, Ar), 6.35 (1H, d, Ar), 6.38 (1H, d, Ar) 6.52 (1H, s, Ar), 6.55 (1H, s, Ar), 7.03 (2H, m, Ar), 7.08 (1H, m, Ar), 7.47−7.58 (4H, m, Ar), 7.95 (1H, m, Ar). ^{31}P{^{1}H} NMR (CD_3OD): δ = 18.6. MS: calculated 654.3, observed 654.3 (M^+)

Preaparation of Rhodamine−PPA. Conjugate rhodamine−PPEt$_2$ (100 mg, 0.153 mmol) was dissolved in dry MeCN (5 mL), and trimethylsilyl bromide (612 mg, 4 mmol) was added. The reaction mixture was stirred at room temperature in the dark for 12 h. Volatiles were evaporated on a rotavap. EtOH (10 mL) was added to the nonvolatile residue, and the resulting solution was evaporated on a rotavap. The procedure was repeated three times. The product was obtained in the form of a purple solid (89 mg, 97%, purity of >95% according to elemental analysis) and was not further purified. EA found: C, 57.11; H, 5.90; N, 5.85; Br 10.99, 4.08. Calcd for $C_{34}H_{42}BrN_3O_7P^+$: C, 57.06; H, 5.92; N, 5.87; Br, 11.17. ^{1}H NMR (CD_3OD): δ = 1.16 ppm (12H, t, CH_3), 3.71 ppm (8H, q, CH_2), 6.78 ppm (2H, dd, Ar), 7.25 ppm (2H, d, Ar), 7.37 ppm (1H, m, Ar), 7.44 ppm (2H, dd, Ar), 7.55 ppm (2H, dd, Ar), 7.66 ppm (2H, d, Ar), 7.76 ppm (2H, m, Ar), 8.09 ppm (1H, m, Ar). ^{31}P{^{1}H}NMR (CD_3OD): δ = 14.1 ppm (1P, s). ^{13}C{^{1}H} NMR (CD_3OD): δ = 10.8 ppm (4C, s, CH_3), 54.9 ppm (4C, s, CH_2), 95.3 (1C, s, Ar) 113.2 (2C, s, Ar), 120.0 (2C, s, Ar), 123.0 (2C, s, Ar), 125.4 (2C, d, Ar), 128.0 (1C, s, Ar), 128.3 (1C, s, Ar), 131.6 (2C, d, Ar), 132.4 (2C, s, Ar), 132.7 (1C, s, Ar), 132.8 (1C, s, Ar), 133.2 (1C, d, Ar), 135.8 (1C, s, Ar), 140.0 (1C, d, Ar), 140.3 (2C, s, Ar), 152.2 (1C, s, Ar), 153.3 (2C, s, Ar), 169.1 (1C, s, C═O). MS: calculated 598.2, observed 596.1 ($M - 2H^+$)

Adsorption of Ln-BPAMD and RPPA onto the TiO_2 Surface. Rhodamine−PPA (2 mg, 3.3 μmol) was dissolved in a 60 mM Gd-BPAMD solution (212 μL, 12 μmol of Gd-BPAMD, pH 2.5). The resulting solution was mixed with 4 mL of TiO_2 colloidal solution. The reaction mixture was stirred at 70 °C for 3 days. The reaction mixture

was dialyzed three times against HCl solution (1 L, pH 2.5) for 12 h to remove excess of sorbate. Then PVA solution (1.33 mL, 66.5 mg of PVA) was added, and the mixture was stirred in the vial for 12 h. Then the reaction mixture was dialyzed three times against pure water (1 L) for 12 h. The resulting pH was around 6.5.

Experiments with Stem Cells. To isolate rat bone marrow stromal cells (rMSCs), femurs were dissected from 4-week-old Wistar rats. The ends of the bones were cut, and the marrow was extruded with 5 mL of Dulbecco's modified Eagle's medium (DMEM) with L-glutamine (PAA, Pasching, Austria) using a needle and syringe. Marrow cells were plated in 80 cm^2 tissue culture flasks in DMEM/10% fetal bovine serum (FBS) with 100 U/mL penicillin and 0.1 mg/mL streptomycin. After 24 h, the nonadherent cells were removed by replacing the medium. The medium was changed every 2−3 days as the cells grew to confluence. The cells were lifted by incubation with 0.25 wt % trypsin solution.

Human MSCs (hMSCs) were obtained from Bioinova, s.r.o. Cells were plated in a 75 cm^2 tissue culture flask and cultured under the same culture conditions as rMSC.

Cell Labeling and Cell Viability. rMSCs, at 100 000 cells/mL medium, were cultured in a 12-well culture dish in a culture medium containing TiO_2@RhdGd agent (0.21 mg/mL) for 48 h. The nanoparticles were washed out by PBS. Cells were harvested by trypsin/EDTA (Invitrogen) and counted. The viability of rMSCs was determined using the trypan blue exclusion test (0.1 wt %). To measure the effect of TiO_2@RhdGd agent on growth and proliferation of hMSCs, we used the xCELLigence real time cell analyzer (RTCA) instrument. An amount of 10 000 h MSCs per well was seeded in E-Plates 16 in quadruplicate in normal culture medium or in medium containing TiO_2@RhdGd agent from the beginning of experiment or with addition of TiO_2@RhdGd agent after 6 h, when the proliferation curve has reached plateau. The final volume of each well was 200 μL. Dynamic cell proliferation was monitored at 15 min intervals from time of plating until the end of the experiment (53 h). The cell index value (dimensionless parameter) was derived from the change in electrical impedance as the living cells interact with the biocompatible microelectrode surface in the E-Plate well.

Labeling Efficiency. To check the intensity of fluorescent staining, an Axioplan Imaging II fluorescence microscope was used at a magnification of 200×. Cell nuclei were labeled with DAPI (Sigma, 100 μL/ml). Labeling efficiency was determined by manually counting the total number of cell nuclei and cell nuclei in fluorescent cells in 10 optical fields from three wells. The scanned images with manually labeled cells were processed by the image analysis toolbox of MATLAB software (The MathWorks, MA, U.S.). The presence or absence of a label inside the cells was expressed as the percentage of labeled cells.

MRI Visualization of Labeled Stem Cells. About 10^6 cells were labeled for 48 h, as is described above. After this time, the cells were harvested and counted in a Bürker chamber. The cell suspensions were transferred to 1.5 mL vials. The suspensions were centrifuged at 3000*g*, and then the vials were put into wells previously filled with 4% gelatin stabilized by 0.1% phenol and 0.1% NaN_3. Magnetic resonance measurements were performed using a 4.7 T Bruker Biospec spectrometer equipped with a commercially available resonator coil (Bruker) at 25 °C. A standard T_1-weighted turbo spin echo sequence (repetition time T_R = 250 ms, TE = 12 ms, slice thickness = 0.63 mm, turbo factor = 1, number of acquisitions = 8, FOV = 4 × 4 cm^2, matrix = 256 × 256) was used.

Experiments with HeLa Cells. *Cell Culture Incubation. Standard Procedure.* HeLa cells were grown in Dulbecco's modified Eagle medium (DMEM, Gibco BRL, Scotland) up to 80% confluency, supplemented with 10% fetal inactivated bovine serum (FBS, Gibco BRL, Scotland), 40 mg/mL gentamycin (Lek, Slovenia), 0.25 mg/mL glutamine (Sevapharma, Czech Republic) and incubated in the presence of TiO_2@RhdGd nanoparticles (0.21 mg/mL, 37 °C, 5% CO_2, 24 h).

Characterization of the Nanoparticle Toxicity. Cells were incubated according to the standard procedure and consequently were harvested using 0.5 mL of trypsine/EDTA solution in PBS. Cells released into suspension were merged with the nonadherent ones floating in the incubation medium collected previously. The mixture was stained with DAPI distinguishing the living and the dead cells and analyzed by the flow cytometer LSR II (Becton Dickinson). Data were analyzed using BD Diva software measuring the mean fluorescence intensity of the cells in the Cy5 channel as well. Numbers of events for the unambiguously living NL and the unambiguously dead cells ND were recorded, whereas the viability was determined as the NL/(NL + ND) ratio.

Colocalization of Nanoparticles with Endosomal Marker. Coverslips with cells, incubated according to standard procedure, were co-incubated with 5 μg/mL holotransferrin-FITC (EXBIO) for 30 min to saturate appropriate early and recycling endosomes with the corresponding fluorescence signal. After relevant treatments, coverslips with approximately 500 000 cells were rinsed twice with PBS (0.01 M PBS, pH 7.4) and fixed with 3.8% formaldehyde in PBS (room temperature, 20 min, directly in the multiwell plate). Fixation was followed by washing with PBS, neutralization with 0.015 M NH_4Cl in PBS, and mounting in Mowiol containing DAPI (1 μg/50 mL).

Colocalization of Nanoparticles with Lysozomal Marker. Coverslips with cells, incubated according to standard procedure, were permeabilized using 0.1% Triton X-100 first, blocked with 2% BSA in PBS, incubated with mouse anti-LAMP-1 antibody (1:1000, Santa Cruz, CA) in 1% BSA in PBS and with the secondary goat anti-mouse Alexa Fluor 488 (1:1000, Molecular Probes) labeled antibody. Specimens were imaged using an Olympus IX-81 CellR microscope equipped with a Hamamatsu C4742-80-12AG digital camera under a 63× oil-immersion lens.

Illumination with UV Light. Viability Study. Cells cultivated and incubated according to standard procedure were washed in PBS (medium was collected so that no dead cells were lost) and illuminated for 7, 15, or 20 min with UV light (mercury black lamp, glass filter filtering of wavelengths under 350 nm, 5 mW/cm^2, 37 °C). After UV illumination, cells were incubated for 3 h at 37 °C with 5% CO_2 and then harvested using 0.5 mL of trypsine/EDTA solution in PBS (trypsin was inactivated after cells were detached from the plastic using previously collected FBS containg medium from the same cell cultures). Cell suspesion was stained with DAPI distinguishing the living and the dead cells and analyzed by the flow cytometer LSR II. The experiment was repeated two times in triplicate.

In Vivo Experiment. Primary B and T lymphocytes together with antigen presenting cells (APC) from the lymph node were prepared from 6-week-old Bl-6 mouse. The lymph node was dissected, and the cells were mechanically homogenyzed before being transferred to RPMI (medium supplemented with 10% fetal inactivated bovine serum (FBS and RPMI, Gibco BRL, Scotland), 40 mg/mL gentamycin (Lek, Slovenia), 0.25 mg/mL glutamine (Sevapharma, Czech Republic)) and incubated with the nanoparticles (0.21 mg/mL, 37 °C, 5% CO_2, 24 h). After incubation cells were washed with RPMI twice and 3 × 10^6 viable lymph node derived leukocytes were transferred in the recipient Bl-6 mice via caudal vein. After 12 h, the recipient mouse was dissected, inguinal lymph nodes were extracted and immediately quickly imaged using a motorized fluorescence binolupe (Zeiss Lumar, V12). The same lymph nodes were fixed (3.8% PFA in phosphate buffered saline (PBS), 1 h), transferred to 20% sucrose (in PBS solution, 4 °C, 2 h frozen (−18 °C) in tissue freezing medium Jung (Leica Microsystems) on metal specimen disk, and cut at 15 μm with Leica CM 3050S cryocut. Thermo Scientific Superfrost Plus microscope slides were used (Menzel-Glaser). The cells on the slides were permeabilized in 0.1% Triton X-100 and mounted in Mowiol-DAPI.

■ ASSOCIATED CONTENT

Supporting Information. Additional details on hydrolytical stability of TiO_2@RhdGd, on derivation of per particle relaxivity, and on proliferation curves of human mesenchymal

stem cells. This material is available free of charge via the Internet at http://pubs.acs.org.

AUTHOR INFORMATION

Corresponding Author

*Phone: +420221951259. Fax: +420221951253. E-mail: lukes@natur.cuni.cz.

ACKNOWLEDGMENT

We thank our co-workers from Heyrovsky Institute of Physical Chemistry Jaromír Jirkovský and Michal Kolář for providing TiO_2 nanoparticles. We also thank Magdalena Krulova for work with mice during in vivo experiments. Support from the Ministry of Education of the Czech Republic (Grants MSM0021620857 and SVV 261206/2010) is acknowledged. V.K. thanks RP MSMT 14/63 for support. This work was carried out in the framework of COST D38 Action (MŠMT OC179).

ABBREVIATIONS USED

CA, contrast agent; TiO_2@RhdGd, TiO_2 nanoparticles modified with Gd(III) complex and fluorescent dye; MRI, magnetic resonance imaging; OI, optical imaging; EPR, enhanced permeability and retention; ICP-AES, inductively coupled plasma atomic emission spectroscopy; MSC, mesenchymal stem cells

REFERENCES

(1) Prokop, A.; Davidson, J. M. Nanovehicular intracellular delivery systems. *J. Pharm. Sci.* **2008**, *97*, 3518–3590.

(2) Etrych, T.; Chytil, P.; Mrkvan, T.; Šírová, M.; Říhová, B.; Ulbrich, K. Conjugates of doxorubicin with graft HPMA copolymers for passive tumor targeting. *J. Controlled Release* **2008**, *132*, 184–192.

(3) Lebdušková, P.; Kotek, J.; Hermann, P.; Vander Elst, L.; Muller, R. N.; Lukeš, I.; Peters, J. A. A gadolinium(III) complex of a carboxylic-phosphorus acid derivative of diethylenetriamine covalently bound to inulin, a potential macromolecular MRI contrast agent. *Bioconjugate Chem.* **2004**, *15*, 881–889.

(4) Rudovský, J.; Botta, M.; Hermann, P.; Hardcastle, K. I.; Lukeš, I.; Aime, S. PAMAM dendrimeric conjugates with a Gd−DOTA phosphinate derivative and their adducts with polyaminoacids: the interplay of global motion, internal rotation, and fast water exchange. *Bioconjugate Chem.* **2006**, *17*, 975–987.

(5) Hrubý, M.; Koňák, C.; Kučka, J.; Větřík, M.; Filippov, S. K.; Větvička, D.; Macková, H.; Karlsson, G.; Edwards, K.; Říhová, B.; Ulbrich, K. Thermoresponsive, hydrolytically degradable polymer micelles intended for radionuclide delivery. *Macromol. Biosci.* **2009**, *9*, 1016–1027.

(6) Michalet, X.; Pinaud, F. F.; Bentolila, L. A.; Tsay, J. M.; Doose, S.; Li, J. J.; Sundaresan, G.; Wu, A. M.; Gambhir, S. S.; Weiss, S. Quantum dots for live cells, in vivo imaging, and diagnostics. *Science* **2005**, *307*, 538–544.

(7) Eljamel, M. S. Fluorescence image-guided surgery of brain tumors: explained step-by-step. *Photodiagn. Photodyn. Ther.* **2008**, *5*, 260–263.

(8) Trehin, R.; Figueiredo, J.-L.; Pittet, M. J.; Weissleder, R.; Josephson, L.; Mahmood, U. Fluorescent nanoparticle uptake for brain tumor visualization. *Neoplasia* **2006**, *8*, 302–311.

(9) Kotková, Z.; Kotek, J.; Jirák, D.; Jendelová, P.; Herynek, V.; Berková, Z.; Hermann, P.; Lukeš, I. Cyclodextrin-based bimodal fluorescence/MRI contrast agents: an efficient approach to cellular imaging. *Chem.—Eur. J.* **2010**, *16*, 10094–10102.

(10) Kříž, J.; Jirák, D.; White, D.; Foster, P. Magnetic resonance imaging of pancreatic islets transplanted into the right liver lobes of diabetic mice. *Transplant. Proc.* **2008**, *40*, 444–448.

(11) *The Chemistry of Contrast Agents in Medical Magnetic Resonance Imaging*; Merbach, A. E., Tóth, É., Eds.; Wiley: Chichester, U.K., 2001.

(12) Rieter, W. J.; Kim, J. S.; Taylor, K. M. L.; An, H.; Lin, Wei.; Tarrant, T.; Lin, W. Hybrid silica nanoparticles for multimodal imaging. *Angew. Chem., Int. Ed.* **2007**, *46*, 3680–3682.

(13) Carniato, F.; Tei, L.; Cossi, M.; Marchese, L.; Botta, M. A chemical strategy for the relaxivity enhancement of Gd^{III} chelates anchored on mesoporous silica nanoparticles. *Chem.—Eur. J.* **2010**, *16*, 10727–10734.

(14) Tsotsalas, M.; Busby, M.; Gianolio, E.; Aime, S.; De Cola, L. Functionalized nanocontainers as dual magnetic and optical probes for molecular imaging applications. *Chem. Mater.* **2008**, *20*, 5888–5893.

(15) Prinzen, L.; Miserus, R.-J. J. H. M.; Dirksen, A.; Hackeng, T. M.; Deckers, N.; Bitsch, N. J.; Megens, R. T. A.; Douma, K.; Heemskerk, J. W.; Kooi, M. E.; Frederik, P. M.; Slaaf, D. W.; van Zandvoort, M. A. M. J.; Reutelingsperger, C. P. M. Optical and magnetic resonance imaging of cell death and platelet activation using annexin A5-functionalized quantum dots. *Nano Lett.* **2007**, *7*, 93–100.

(16) Mulder, W. J. M.; Strijkers, G. J.; Van Tilborg, G. A. F.; Cormode, D. P.; Fayad, Z. A.; Nicolay, K. Nanoparticulate assemblies of amphiphiles and diagnostically active materials for multimodality imaging. *Acc. Chem. Res.* **2009**, *42*, 904–914.

(17) Gerion, D.; Herberg, J.; Bok, R.; Gjersing, E.; Ramon, E.; Maxwell, R.; Kurhanewicz, J.; Budinger, T. F.; Gray, J. W.; Shuman, M. A.; Chen, F. F. Paramagnetic silica-coated nanocrystals as an advanced MRI contrast agent. *J. Phys. Chem. C* **2007**, *111*, 12542–12551.

(18) Koole, R.; van Schooneveld, M. M.; Hilhorst, J.; Castermans, K.; Cormode, D. P.; Strijkers, G. J.; de Mello Donega, C.; Vanmaekelbergh, D.; Griffioen, A. W.; Nicolay, K.; Fayad, Z. A.; Meijerink, A.; Mulder, W. J. M. Paramagnetic lipid-coated silica nanoparticles with a fluorescent quantum dot core: a new contrast agent platform for multimodality imaging. *Bioconjugate Chem.* **2008**, *19*, 2471–2479.

(19) Zhang, Z.; Berns, A. E.; Willbold, S.; Buitenhuis, J. Synthesis of poly(ethylene glycol) (PEG)-grafted colloidal silica particles with improved stability in aqueous solvents. *J. Colloid Interface Sci.* **2007**, *310*, 446–455.

(20) Endres, P. J.; Paunesku, T.; Vogt, S.; Meade, T. J.; Woloschak, G. E. DNA−TiO_2 nanoconjugates labeled with magnetic resonance contrast agents. *J. Am. Chem. Soc.* **2007**, *129*, 15760–15761.

(21) Thurn, K. T.; Paunesku, T.; Wu, A.; Brown, E. M. B.; Lai, B.; Vogt, S.; Maser, J.; Aslam, M.; Dravid, V.; Bergan, R.; Woloschak, G. E. Labeling TiO_2 nanoparticles with dyes for optical fluorescence microscopy and determination of TiO_2-DNA nanoconjugate stability. *Small* **2009**, *5*, 1318–1325.

(22) Salih, F. M. Enhancement of solar inactivation of *Escherichia coli* by titanium dioxide photocatalytic oxidation. *J. Appl. Microbiol.* **2002**, *92*, 920–926.

(23) Farshbaf Dadjour, M.; Ogino, C.; Matsumura, S.; Nakamura, S.; Shimizu, N. Disinfection of *Legionella pneumophila* by ultrasonic treatment with TiO2. *Water Res.* **2006**, *40*, 1137–1142.

(24) Rozhkova, E. A.; Ulasov, I.; Lai, B.; Dimitrijevic, N. M.; Lesniak, M. S.; Rajh, T. A high-performance nanobio photocatalyst for targeted brain cancer therapy. *Nano Lett.* **2009**, *9*, 3337–3342.

(25) Cai, R.; Kubota, Y.; Shuin, T.; Sakai, H.; Hashimoto, K.; Fujishima, A. Induction of cytotoxicity by photoexcited TiO_2 particles. *Cancer Res.* **1992**, *52*, 2346–2348.

(26) Lai, T.-Y.; Lee, W.-C. Killing of cancer cell line by photoexcitation of folic acid-modified titanium dioxide nanoparticles. *J. Photochem. Photobiol., A* **2009**, *204*, 148–153.

(27) Ivanković, S.; Gotić, M.; Jurin, M.; Musić., S. Photokilling squamous carcinoma cells SCCVII with ultrafine particles of selected metal oxides. *J. Sol-Gel Sci. Technol.* **2003**, *27*, 225–233.

(28) Huang, N.-P.; Xu, M.-H.; Yuan, C.-W.; Yu, R.-R. The study of the photokilling effect and mechanism of ultrafine TiO_2 particles on U937 cells. *J. Photochem. Photobiol., A* **1997**, *108*, 229–233.

(29) Kalbáčová, M.; Macak, J. M.; Schmidt-Stein, F.; Mierke, C. T.; Schmuki, P. TiO_2 nanotubes: photocatalyst for cancer cell killing. *Phys. Status Solidi RRL* **2008**, *2*, 194–196.

(30) Řehoř, I.; Kubíček, V.; Kotek, J.; Hermann, P.; Lukeš, I.; Száková, J.; Elst, L. V.; Muller, R. N.; Peters, J. A. ^1H NMR relaxivity of aqueous suspensions of titanium dioxide nanoparticles coated with a gadolinium(III) chelate of a DOTA-monoamide with a phenylphosphonate pendant arm. *J. Mater Chem.* **2009**, *19*, 1494–1500.

(31) Řehoř, I.; Kubíček, V.; Kotek, J.; Hermann, P.; Száková, J.; Lukeš, I. Modification of nanocrystalline TiO_2 with phosphonate- and bis(phosphonate)-bearing macrocyclic complexes: sorption and stability studies. *Eur. J. Inorg. Chem.* **2011**, 1981–1989.

(32) Kubíček, V.; Rudovský, J.; Kotek, J.; Hermann, P.; Elst, L. V.; Muller, R. N.; Kolar, Z. I.; Wolterbeek, H. T.; Peters, J. A.; Lukeš, I. A bisphosphonate monoamide analogue of DOTA: a potential agent for bone targeting. *J. Am. Chem. Soc.* **2005**, *127*, 16477–16485.

(33) Vitha, T.; Kubíček, V.; Hermann, P.; Kolar, Z. I.; Wolterbeek, H. T.; Peters, J. A.; Lukeš, I. Complexes of DOTA-bisphosphonate conjugates: probes for determination of adsorption capacity and affinity constants of hydroxyapatite. *Langmuir* **2008**, *24*, 1952–1958.

(34) Kubíček, V.; Vitha, T.; Kotek, J.; Hermann, P.; Vander Elst, L.; Muller, R. N.; Lukeš, I.; Peters, J. A. Towards MRI contrast agents responsive to Ca(II) and Mg(II) ions: metal-induced oligomerization of dota-bisphosphonate conjugates. *Contrast Media Mol. Imaging* **2010**, *5*, 294–296.

(35) Powell, D. H.; Dhubhghaill, O. M. N.; Pubanz, D.; Helm, L.; Lebedev, Y. S.; Schlaepfer, W.; Merbach, A. E. Structural and dynamic parameters obtained from ^{17}O NMR, EPR, and NMRD studies of monomeric and dimeric Gd^{3+} complexes of interest in magnetic resonance imaging: an integrated and theoretically self-consistent approach. *J. Am. Chem. Soc.* **1996**, *118*, 9333–9346.

(36) Livramento, J. B.; Tóth, É.; Sour, A.; Borel, A.; Merbach, A. E.; Ruloff, R. High relaxivity confined to a small molecular space: a metallostar-based, potential MRI contrast agent. *Angew.Chem., Int. Ed.* **2005**, *44*, 1480–1484.

(37) Kraitchman, D. L.; Gilson, W. D.; Lorenz, C. H. Stem cell therapy: MRI guidance and monitoring. *J. Magn. Reson. Imaging* **2008**, *27*, 299–310.

(38) Arbab, A. S.; Frank, J. A. Cellular MRI and its role in stem cell therapy. *Regener. Med.* **2008**, *3*, 199–215.

(39) Hirao, T.; Masunaga, T.; Ohshiro, Y.; Agawa, T. A novel synthesis of dialkyl arenephosphonates. *Synthesis* **1981**, *1*, 56–57.

(40) Kolář, M.; Měšťánková, H.; Jirkovský, J.; Heyrovský, M.; Šubrt, J. Some aspects of physico-chemical properties of TiO_2 nanocolloids with respect to their age, size, and structure. *Langmuir* **2006**, *22*, 598–604.